AIAA JOURNAL
Vol. 31, No. 3, March 1993

Comparison of Excitation Techniques for Quantitative Fluorescence Imaging of Reacting Flows

Jerry M. Seitzman* and Ronald K. Hanson†
Stanford University, Stanford, California 94305

To determine the quantitative limitations of fluorescence imaging of OH, various systematic and random errors associated with three excitation approaches are analyzed. The three laser pumping schemes, 1) dye laser excitation of the $A^2\Sigma^+ \leftarrow X^2\Pi$ (1,0) band, 2) KrF laser excitation of the predissociative (3,0) band, and 3) saturated pumping of the (0,0) band with a XeCl laser, are compared to find which method minimizes the overall error. The approaches are compared by calculating shot-noise limited random errors and systematic deviations between the standard scaling equations and solutions to a time-dependent five-level rate equation model of the population densities. The model is used to address saturation and depletion (bleaching) effects. Dye laser excitation has the lowest overall error for single-shot imaging in turbulent hydrocarbon-air and hydrogen-air flames. XeCl pumping produces the strongest signals, with evidence of strong saturation and ground state depletion effects. KrF pumping of the weakly absorbing and predissociative (3,0) band shows potential for quantitative imaging, when frame averaging is used.

Introduction

PLANAR imaging is a powerful tool for obtaining spatially correlated flowfield information at an instant in time. Thus planar imaging has proven an effective tool for locating flames, regions of burned or unburned gases, recirculation zones, shock waves, large-scale structures, and other features.[1] In addition, planar imaging provides the capability of delivering quantitative information at multiple flowfield points. Planar laser-induced fluorescence (PLIF) is particularly attractive owing to the strength of the process, relative to its primary competitors, Rayleigh and Raman scattering, and to its potential for monitoring several flowfield parameters: species concentration, temperature, velocity and pressure.[2] Thus, advances in PLIF which provide more quantitative data have high potential to generate a better understanding of both reacting and nonreacting flows.

In a typical PLIF measurement, an excited electronic state of a molecule is populated by a laser source with an emission frequency tuned to an optically allowed resonance between the excited state and a lower energy state. Excited molecules can then emit light, fluoresce, producing the PLIF signal. To date, collisional quenching of the excited state has been considered the major limitation to quantitative PLIF measurements, as collision rates depend on local chemical and thermodynamic parameters. Various laser pumping schemes have been suggested to reduce the importance of collisional quenching and produce more quantitative images. It should be noted, however, that in many cases the variation in quench rate across a region is small or can be modeled to some accuracy. To be considered an improvement, therefore, the errors associated with the alternate pumping schemes should be less than the systematic errors associated with quenching variations.

Here, we examine various error sources, both systematic and random, for three different laser pumping methods: the standard linear pumping technique; predissociated PLIF, in which the upper state decay rate is partially controlled by molecular dissociation; and saturated pumping, with laser stimulated emission limiting the decay rate. The systematic errors arise from unmeasured variations in parameters which affect the fluorescence or from failings in the predictive nature of the standard steady-state fluorescence models. In low light level PLIF imaging, the primary source of random error is signal shot noise, which is signal level dependent. By comparing the combined errors for the three pumping schemes, the technique with the smallest overall error in a given flowfield can be determined.

In the present comparison, we consider hydroxyl (OH) imaging in turbulent hydrocarbon-air and hydrogen-air flames. Turbulent combustion, which dominates many practical propulsion and energy conversion devices, presents a particularly challenging application for diagnostic methods. In addition, the crucial role played by large organized structures, for example, in controlling mixing and dissipation rates, has recently been recognized. The measurement of instantaneous spatial structures is therefore essential for verifying various combustion models. The OH radical was chosen for this comparison because of its importance in flame chemistry, because of its ability to mark specific regions of the flow, and because it has relatively well-established spectroscopic and collisional data bases. In premixed hydrocarbon flames, quenching of OH varies by less than 10% across regions of significant OH concentration.[3,4] In methane diffusion flames, proper choice of transitions allow uncorrected LIF measurements of OH to be within $\pm 10\%$ of the actual value of the OH concentration near the reaction zone.[5] In other cases, measurement of some parameters, such as temperature and velocity, can be made by taking ratios of fluorescence images in a way that cancels or significantly reduces the collisional quenching dependence.[6,7] It is against this backdrop that other error sources are compared.

Systematic Errors: Scaling Models

As previously detailed, the laser in a typical PLIF measurement causes molecules to be transferred from a specific rotation-vibration energy level in the ground electronic state to another discrete level in a higher energy electronic state. After excitation, various decay processes affect the laser-populated upper state. For example, the molecule can be returned to its original state by (laser-induced) stimulated emission. In addition, inelastic collisions with other molecules produce rotational and vibrational energy transfer, and also electronic energy transfer or quenching. In some cases, dissociation of the molecule can be produced by a "collisionless" transition from a stable to a repulsive electronic arrangement in the molecule,

Received March 20, 1992; revision received May 13, 1992; accepted for publication June 5, 1992.

*Research Associate, High Temperature Gasdynamics Laboratory, Department of Mechanical Engineering. Member AIAA.

†Professor, High Temperature Gasdynamics Laboratory, Department of Mechanical Engineering. Senior Member AIAA.

which is known as predissociation. Finally, the originally populated state, and nearby states indirectly populated through collisions, can fluoresce, producing the PLIF signal.

The fluorescence signal is usually modeled by solving a set of rate equations for the populations of the various energy levels of the molecule. The simplest model uses only the two laser-coupled energy levels and is a steady-state solution. The fluorescence equations derived from this model are generally used to interpret PLIF images and to apply corrections owing to systematic effects such as a laser sheet's spatially nonuniform energy profile.

According to this model for a weak (nonperturbing) laser pulse, the total number of photons N_p striking a photodetector from a collection volume V_c imaged onto the detector is[2]

$$N_p = \eta \frac{\Omega}{4\pi} f_1(T)\, n_a V_c B_{12} E_\nu \frac{A_{21}}{A_{21} + Q_{21}} \tag{1}$$

where η is the transmission efficiency of the collection optics, Ω the collection solid angle, $f_1(T)$ the fractional (Boltzmann) population of the lower laser coupled state in the absence of the laser field, n_a the number density of the absorbing species, and E_ν (J cm^{-2} Hz^{-1}) the spectral fluence of the laser. Additionally, it is assumed the fluorescence is emitted equally into 4π sr and the laser spectral width is broad compared to the bandwidth of the molecular transition.

For fully saturated fluorescence, the number of signal photons would instead be given by[2]

$$N_p = \eta \frac{\Omega}{4\pi} f_1(T)\, n_a V_c \Delta t \frac{A_{21}}{1 + g_1/g_2} \tag{2}$$

where g_1 and g_2 are the degeneracies of the two laser coupled levels and Δt is the effective fluorescence integration time. When coupling to the other populated energy levels is considered, the population fraction term in Eq. (2) can approach unity.[8]

Since these equations or similar ones are used to guide conversion of PLIF images to field measurements of flow variables such as concentration or temperature, deviations of the actual signal from these models will typically represent a source of systematic error. The inaccuracies of the standard equations can be estimated by comparing their predictions to the results from a time-dependent numerical solution of the rate equations. We consider the five-level system depicted in Fig. 1. Similar models have been examined to study the difference in saturation effects between molecular systems and atomic systems, for which two-level models are more pertinent.[8,9]

Levels 1 and 2 represent rovibronic states directly coupled by the laser. Level 4 represents a bath of other rotational energy levels in the same vibrational state, which can exchange population with the absorbing level, 1. Likewise, level 3 is the bath for the excited state. Level 5 accounts for predissociated molecules and for molecules which are electronically quenched to vibrational levels other than the bath level 4. It is assumed that vibrational transfer in the ground electronic state is slow, such that none of these molecules return to the absorbing bath during the laser pulse.

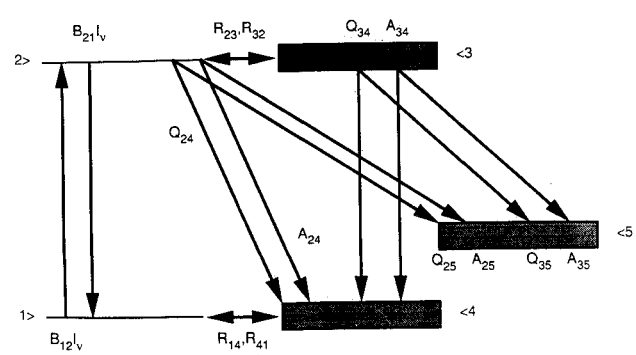

Fig. 1 Energy level schematic for five-level PLIF model, levels 1 and 2 are coupled by the laser, 4 and 3 are their respective bath levels, and level 5 acts as a sink: various processes represented include $B_{ij}I_\nu$, laser stimulated rates; Q_{ij}, collisional quench rates; A_{ij}, spontaneous emission rates; and R_{ij}, rotational transfer rates.

It must also be noted that the rates R_{41} and R_{32} are not elementary rate coefficients, but depend on the population distribution of the bath, i.e., $n_4 R_{41} = \Sigma n_b r_{b1}$ or $R_{41} = \Sigma f_b r_{b1}$, where r_{b1} is the rate coefficient for collisional transfer from rotational energy level b in the bath and f_b is its relative population. For weak laser pumping and fast rotational transfer, R_{41} and R_{32} closely approach the rates associated with Boltzmann rotational distributions.

Also included in the model is the actual spectral overlap between the laser profile (ϕ_L) and the Doppler-, collision-,[10] and lifetime-broadened absorption profile (ϕ_a) of the molecule, i.e.,

$$g(\nu_L) = \int_{-\infty}^{\infty} \phi_L(\nu, \nu_L)\phi_a(\nu, \nu_a)\, d\nu \tag{3}$$

where ν_L is the center frequency of the laser and ν_a the center frequency of the molecular absorption transition. For the present comparisons, the laser is modeled with a Gaussian line shape and the molecular absorption transition is given by a Voigt profile. The effect of the overlap integral is to replace the laser stimulated rates, $B_{ij}I_\nu$ (see Fig. 1) by $B_{ij}Ig(\nu_L)$, where I is the total laser intensity. As written, the overlap integral (3) is valid except for inhomogeneous saturation effects.[11]

Random Errors: Noise

The signal-to-noise ratio (SNR) of PLIF images acquired with a typical intensified, solid-state camera system is given by[12]

$$\text{SNR} = \frac{N_p \eta_{pc} G_e}{[N_p \eta_{pc} G_e (G_e K + 1) + N_x^2]^{1/2}} \tag{4}$$

where η_{pc} is the quantum efficiency of the photocathode, G_e the overall electron gain (array detector electrons/photocathode electrons), K a noise factor associated primarily with the electron gain of the intensifier (typically, the lowest value of K for an intensifier is between 1 and 3), and N_x the combined readout, dark and digitization noise of the camera system. The first term in the denominator of Eq. (3) represents the signal shot noise. When the shot-noise term dominates the camera noise term, the signal is shot-noise limited and the SNR is given by

$$\text{SNR} = (N_p \eta_{pc}/K)^{1/2} \tag{5}$$

assuming, as is usually the case, $G_e K \gg 1$.

Laser Pumping Options for OH PLIF

Laser-induced fluorescence of OH is most often performed using the $A^2\Sigma^+ \leftarrow X^2\Pi(v'' = 0)$ system, with transition wavelengths below approximately 320 nm. For excitation from the $X^2\Pi(v'' = 0)$ state, the (0,0) band has the highest transition probabilities[13] and was used in many of the original PLIF measurements.[14,15] In the absence of collision-induced vibrational excitation in the upper state, practically all of the fluorescence is re-emitted in the (0,0) band. Thus, fluorescence trapping, absorption of the emitted OH fluorescence by other OH molecules, and elastic laser scattering can be problems in some imaging measurements.

Excitation of the (1,0) band near 282 nm combined with detection of the strong (1,1) band near 315 nm has been used to avoid these problems.[15,16] The stimulated absorption coefficient for the (1,0) band (B_{10}) is only slightly lower than that for the (0,0) band, $B_{10}/B_{00} \cong 0.3$. For these approaches, frequency doubled dye lasers are the typical illumination sources. Because of the limited pulse energies (~1-30 mJ) available from

these sources, the resulting fluorescence measurements are usually considered to fall in the linear fluorescence regime.

The recent introduction of tunable excimer lasers has resulted in new pumping options for OH PLIF. Specifically, commercially available XeCl lasers, which emit near 308 nm, and KrF excimers, operating around 248 nm, provide pulse energies in excess of 100 mJ. With tuning ranges of roughly 1 nm, these two lasers can excite a limited number of OH lines.[17,18] The high pulse energies of the XeCl at 308 nm allow for high signal levels and suggest the potential for saturated fluorescence imaging of the (0,0) band in atmospheric pressure flames.

The more powerful KrF laser permits imaging of OH using the (3,0) band, which has a relatively weak transition probability, $B_{30}/B_{00} \cong 0.006$ (Ref. 13). As with the (1,0) pumping, a significant proportion of the fluorescence occurs in red-shifted vibrational bands, e.g. (3,1), (3,2), and (3,3). Additionally, some of the transitions within the tuning range of the KrF laser have predissociation rates[19] near 10^{10} s^{-1} and may allow quenching-independent PLIF measurements.[20,21] As a potential drawback to predissociated fluorescence measurements, the dissociated O and H atoms will most likely fail to recombine during the short laser pulse (~20 ns), and thus depletion of the ground OH energy levels can occur in the absence of quenching repopulation. Furthermore, interferences from O_2 and H_2O transitions, which can be excited by the KrF laser, as well as photodissociation of water and formation of OH, must be considered.[17,22]

A simple comparison of the expected signal level for these pumping options is illuminating. For the comparison, we consider the following five cases: 1) pumping the $Q_1(5)$ (1,0) line with a pulsed dye laser assuming linear fluorescence; 2) exciting the $Q_1(3)$ (0,0) line with a XeCl laser, assuming linear fluorescence; 3) again exciting the $Q_1(3)$ (0,0) line with a XeCl laser, now assuming saturated fluorescence; 4) pumping the predissociative $P_1(8)$ (3,0) line with a KrF excimer, assuming the steady-state linear fluorescence equation; and 5) also pumping the $P_1(8)$ (3,0) line with a KrF excimer, now assuming enough energy to totally depopulate the ground rotational level with no rotational repopulation. For the (1,0) band, the $Q_1(5)$ line was chosen to obtain good signals without a significant temperature dependence of the Boltzmann population. For the XeCl and KrF options, which can access only a small number of OH lines, the specific rotational lines were chosen based on similar constraints.

Table 1 compares the relative fluorescence, N_p/C, that would be expected for the five pumping options, assuming identical collection optics and detectors. In each case, the temporally integrated fluorescence N_p is proportional to a factor $C = \eta(\Omega/4\pi)\, V_c n_{OH}$, [see Eq. (1)]. Also shown is the shot-noise limited SNR for each approach assuming $\eta = 60\%$, $\Omega/4\pi = 0.0001$ (f 4 collection optics for good spatial resolution; imaging an 80-mm high sheet onto an 18-mm intensifier), $V_c = 0.049$ mm^3 (500-μm sheet width and 256 × 256 pixel array), $n_{OH} = 2.4 \times 10^{16}$ cm^{-3} (0.5% of OH at 1 atm, 1500 K) and $\eta_{pc} = 10\%$. For excitation to $v' = 1$, it is assumed that one-third of the fluorescence comes from the $v' = 0$ state, because of vibrational transfer. For KrF excitation, fluorescence from lower lying vibrational states produced by vibrational transfer from the excited $v' = 3$ (Ref. 17) is omitted, since it would increase the quenching dependence of the fluorescence.

XeCl pumping provides the most intense signals, while the low B coefficient and small fluorescence yield (A/Q) for KrF pumping result in much lower signal levels, even compared to traditional dye laser pumping. The expected KrF signal levels in otherwise identical atmospheric pressure measurements is at least 50 times less than for dye or XeCl pumping.

The fourth column in Table 1, BE_v, is especially noteworthy. In the linear fluorescence limit, BE_v represents the ratio $(\int n_1\, dt)/n_1^0$, the number of times the original population must cycle through level 1 (by quenching or rotational redistribution). In case 1, for example, quenching combined with rotational transfer from nearby rotational levels must effectively resupply the $N = 5$ ($J = 5.5$) state with its original population 16 times. On the other hand, BE_v for XeCl pumping is so large that saturation and possibly bleaching of the ground electronic state are likely.

For predissociative KrF pumping, there is effectively no quenching repopulation. Therefore, signals greater than that possible from the original number of molecules in level 1 can only be achieved by rotational redistribution in the ground levels. Thus, although predissociation has the potential to reduce the dependence of N_p on collisional electronic quenching, the signal can still depend on collisions through rotational transfer in the ground state (and in the upper state, since the predissociation rate in the upper state is also a function of rotational quantum number[19]).

Model Results

The set of rate equations illustrated in Fig. 1 was solved for each of the pumping schemes with a standard ordinary differential equation solver on a personal computer. The flow-field calibration condition is the same one used for the steady-state comparison of Table 1, e.g., 1500 K, 1 atm, 0.5% of OH, total collisional quenching rate Q_e of 0.7×10^9 s^{-1}, with a 80 × 0.5 mm laser sheet. The laser energies and bandwidths, stimulated rate coefficients, and predissociation rates are also identical to those listed in Table 1. At the calibration conditions, the overlap integrals, Eq. (3), are $g_{dye} = 1.50$ cm, $g_{KrF} = 1.33$ cm and $g_{XeCl} = 1.1$ cm.

Additionally, the rotational transfer rate R_{14} is assumed to be the same as R_{23}, which is 10^{10} s^{-1} for the calibration condi-

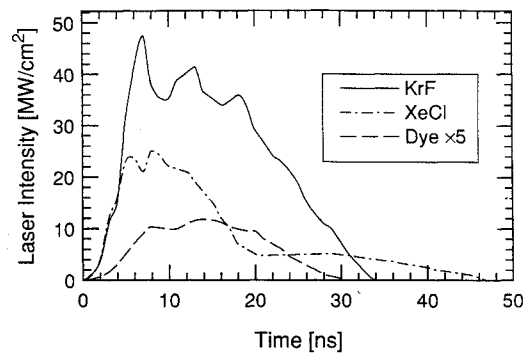

Fig. 2 Temporal profiles for the three pump lasers.

Table 1 Comparison of relative OH fluorescence signals for various pump lasers

Case	Equation for N_p	B, 10^{12} cm^2/Js	BE_v[b]	A, 10^6 s^{-1}	Q 10^9 s^{-1}	f_b^h, %	N_p/C 10^{-4}/pixel	Shot, SNR[j]
1, Dye	$Cf_1 BE_v\,(A/Q)$	9.7	16[c]	1.0	0.7[f]	3.2	7.4	51
2, XeCl	$Cf_1 BE_v\,(A/Q)$	33	370[d]	1.5	0.7[f]	2.9	230	280
3, XeCl	$C(f_1 \rightarrow 1)A\,\Delta t/2$[i]	—[a]	—[a]	1.5	—[a]	2.9	4.4→150	39→230
4, KrF	$Cf_1 BE_v\,(A/Q)$	0.12	4[e]	1.1	11.7[fg]	2.3	0.084	5.4
5, KrF	$Cf_1 A/Q$	—[a]	—[a]	1.1	11.7[fg]	2.3	0.021	2.7

[a]Not applicable. [b]80-mm × 500-μm sheet. [c]10 mJ, 15-GHz bandwidth. [d]100 mJ, 23-GHz bandwidth. [e]200 mJ, 15-GHz bandwidth. [f]Collisional quench rate in 1 atm H_2-air flame. [g]Predissociation rate[20] of 11×10^9 s^{-1}. [h]1500 K. [i]Integration time, $\Delta t = 20$ ns laser pulse. [j]$K = 2$.

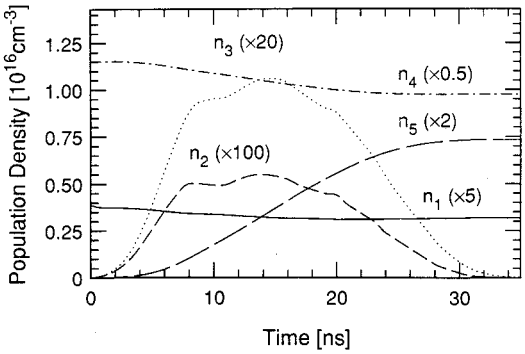

Fig. 3 Temporal development of the population densities for five-level OH model, with 10 mJ of dye laser energy pumping of the $Q_1(5)$ (1,0) line.

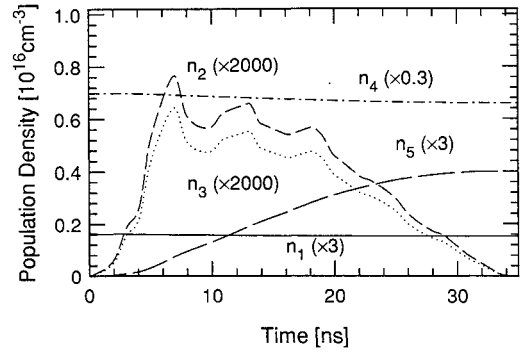

Fig. 4 Temporal development of the five-level model population densities, with a 200 mJ KrF laser pumping the $P_1(8)$ (3,0) line.

tions.[23,24] Finally, the electronic quenching is assumed to be equally divided between transfer to the $v=0$ bath vibrational level (level 4) and to the other vibrational states, that is $Q_{e4} \equiv Q_{24} = Q_{34}$ and $Q_{e5} \equiv Q_{25} = Q_{35}$ are both 0.35×10^9 s^{-1}.

Figure 2 shows the laser temporal profiles used in the calculations. They are measured profiles for Lambda-Physik excimer and excimer-pumped dye lasers. Calculations were also made using the shorter [8 ns full-width at half-maximum (FWHM)] temporal pulse of a Nd:YAG-pumped dye laser and do not significantly vary from the excimer-pumped results presented subsequently. The OH population histories are shown in Figs. 3-5. In all cases, there is some depletion of the laser-pumped level and its bath. For the dye and XeCl pumping, it is produced by quenching to excited vibrational levels, while predissociation plays a key role for KrF pumping. The high laser intensity, large absorption coefficient and assumed quenching ratio ($Q_{e5}/Q_e = \frac{1}{2}$) combine to make depletion effects greatest in the XeCl case. In addition, XeCl pumping is unique in that the laser-coupled levels have almost the same population during the peak of the laser pulse, the traditional definition of saturation.

The population histories of the excited levels (2 and 3) illustrate two differences between predissociative pumping and the other approaches. Because of the high-predissociation rate associated with KrF pumping, the population of the laser-excited rotational level exceeds the bath population and produces over 50% of the fluorescence. On the other hand, significant rotational transfer within the upper levels occurs in both of the other cases, with less than 10% of the fluorescence coming from the initially excited rotational level. In terms of the total population of the two levels, or equivalently the total fluorescence, KrF pumping is at least 100 times less effective than the other two approaches, as expected from the steady-state analysis (Table 1).

To test the predictive accuracy of the steady-state models, Eqs. (1) and (2), the time-dependent analysis was carried out for other laser energies, Boltzmann fractions, and pressures. In each case, the rotational transfer rates and quenching ratio (Q_{e5}/Q_e) were also changed to examine their effect on the model results. Both the fluorescence signal $N_p/[\eta(\Omega/4\pi)V_c]$ and the systematic error resulting from the difference between the simple model's scaling predictions and the time-dependent results were calculated. The error in measuring OH concentration associated with a change in a single variable x, e.g., laser energy, is defined by

$$\text{error} = (n_{OH}^S - n_{OH})/n_{OH}$$
$$= \left[N_p(x)/N_p(x_{cal}) \cdot S(x_{cal})/S(x)\right] - 1 \qquad (6)$$

where n_{OH} is the OH concentration in the volume imaged onto a pixel, n_{OH}^S is the concentration that would be deduced using the simple model to scale the fluorescence from the calibration point, $N_p(x)$ is the fluorescence according to the five-level model, and $S(x)$ is the fluorescence prediction for the simple scaling model. The variable x_{cal} is the calibration value for the variable x at, for example, a point in the flowfield or in another OH source, where conditions are well characterized.

Laser Energy

Figures 6-8 show the effect of laser energy on the fluorescence signal. Some nonlinearities associated with perturbations of the ground state population are seen for all three excitation methods. For the (1,0) dye laser case (Fig. 6), errors as large as 20% are predicted, based on a linear energy dependence. For the calibration conditions, a laser fluence of less than ~10 mJ/cm^2 (4 mJ for the 80×0.5 mm sheet) would be required to ensure linearity within ±5% down to zero energy. As might be expected, increases in the rotational transfer rate (R) and decreases in the ratio Q_{e5}/Q_e tend to reduce the ground state depletion and extend the linear response regime.

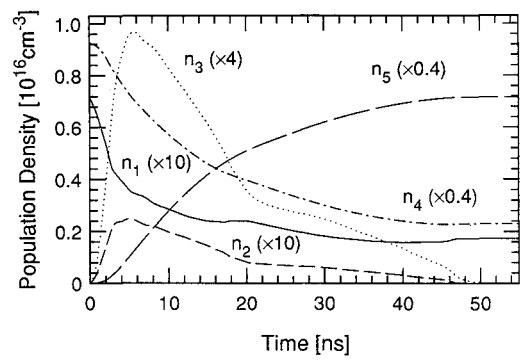

Fig. 5 Temporal development of the five-level model population densities, with 100 mJ of XeCl laser energy pumping the $Q_1(3)$ (0,0) line.

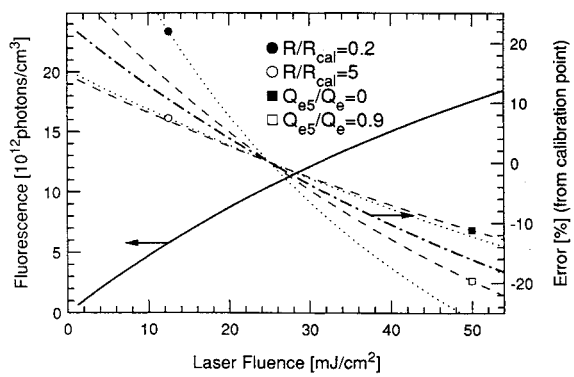

Fig. 6 Variation in the PLIF signal (solid curve) and systematic error (dot-dash curve) with laser energy for dye laser excitation of the $Q_1(5)$ (1,0) line: dotted lines represent error plots for values of R different from the calibration point 10^{10}s^{-1}; the dashed curves show effects of other electronic quench ratios, $(Q_{e5}/Q_e)_{cal} = 0.5$.

As evidenced in Fig. 7, the small B coefficients for (3,0) KrF pumping help limit the ground state depletion, such that a linear energy response is maintained within ±5% up to 400 mJ of pump energy. In this case, variations in the quench ratio have a negligible consequence because of the large predissociative rate. Changes in R still affect ground state depletion, however, and thus the linearity of the fluorescence.

Nonlinear behavior is most severe for XeCl pumping of the (0,0) band (Fig. 8). The flatness of the response at high energies is a product of saturation and depletion of the lower bath level. So in Fig. 8, the errors associated with both the linear [Eq. (1)] and saturated [Eq. (2)] fluorescence models are shown. Now, changes in rotational rates have little consequence (and thus are not shown), while the quench ratio has the larger effect. Because saturation is most pronounced at the peak of the laser pulse, temporal gating of the detector from 3 to 15 ns (see Fig. 2) was studied. Whereas the signal is reduced, the shape of the saturation curve and the error values

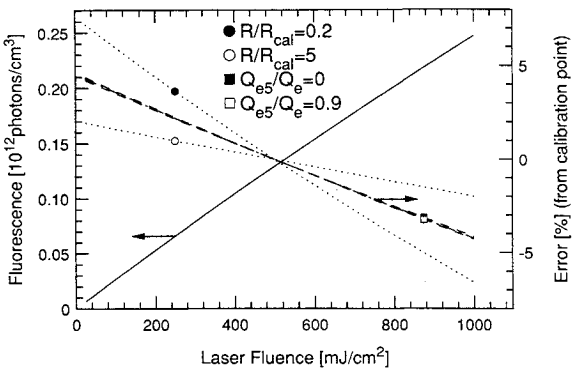

Fig. 7 Variation in PLIF signal with laser energy for KrF laser pumping of the $P_1(8)$ (3,0) line (see Fig. 6 for details).

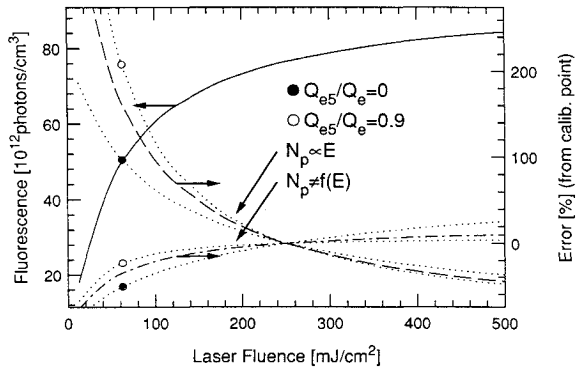

Fig. 8 Variation in PLIF signal with laser energy for XeCl laser excitation of the $Q_1(3)$ (0,0) line: dashed line represents systematic errors associated with the linear model; dot-dashed line is for the saturation model.

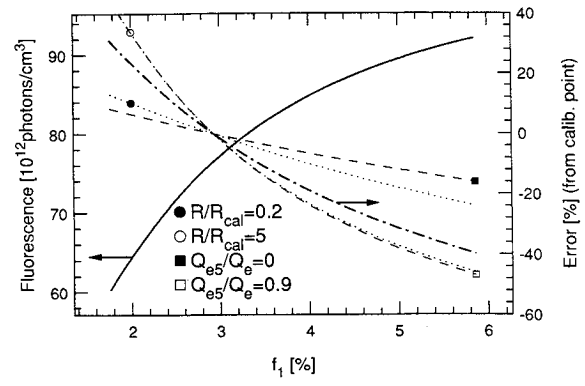

Fig. 9 Variation in the PLIF signal with population fraction of the absorbing state for XeCl laser excitation of the $Q_1(3)$ transition (see Fig. 6 for explanation of the various curves).

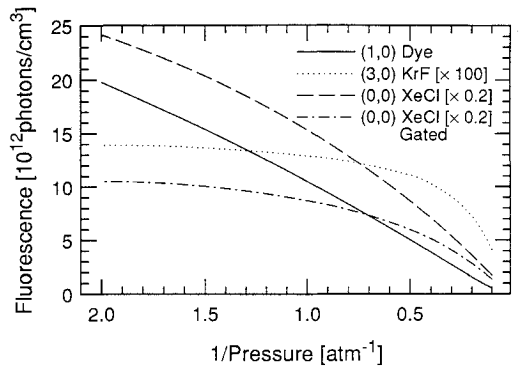

Fig. 10 Variation in OH PLIF signal with pressure for the three pump options; also the result of gating (12 ns) the detector during the peak of the XeCl laser pulse.

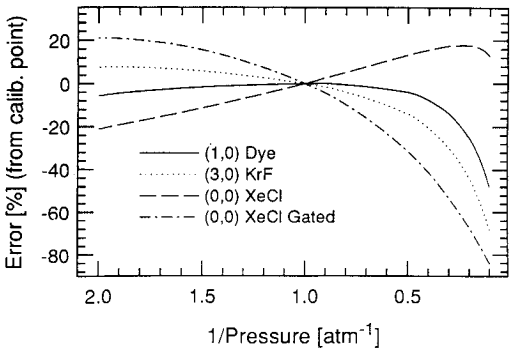

Fig. 11 Systematic errors associated with pressure scaling: $1/P$ scaling for the dye and standard XeCl approaches, pressure-independent scaling for KrF and gated XeCl pumping.

are almost identical to those of Fig. 8. However for the gated case, the error results are more sensitive to variations in R and are comparable to the quench ratio variations shown in Fig. 8.

Population Fraction

As evidenced in the population time histories (Figs. 3–5), some ground state depletion occurs with all three pump lasers and is one source of the nonlinear dependence of the fluorescence signal on laser energy. In addition, this depletion produces a nonlinear response to local changes in the absorbing state's population fraction. Within the scope of the present model and its assumption of negligible ground state vibrational transfer, the depletion is truly a function of population fraction, not ground state number density.

Figure 9 illustrates the effect for the XeCl pump laser. The limits on the initial population fraction (f_1) correspond to Boltzmann distributions ranging from 700 to 2500 K. For XeCl pumping, large errors are associated with linearly scaling the fluorescence with respect to initial population fraction. As shown, decreasing the quench ratio or rotational transfer rate reduces the systematic error. Similar calculations for the dye and KrF cases predict errors not larger than ±5%, again for Boltzmann fractions corresponding to a 700–2500 K range.

Pressure

The pressure dependence of the fluorescence can be important for nonisobaric flows. Pressure changes primarily affect the various collision rates and, therefore, quenching, rotational transfer, and collisional broadening. Figure 10 shows the pressure dependence of the PLIF signal for all three pump options, including XeCl pumping combined with the 12-ns time gating. For the dye and standard XeCl pumping, the fluorescence is primarily inversely proportional to pressure. On the other hand, the signal is nearly independent of pres-

sure, below 1–2 atm, for KrF (predissociation) and gated XeCl (saturation) excitation.

The systematic errors associated with these two scaling laws are displayed in Fig. 11. In general, the dye and KrF methods exhibit the smallest scaling errors. For KrF pumping below ~1.6 atm and below ~2.7 atm for dye pumping, the error is less than 10%. Additionally, KrF and (gated) XeCl pumping have the obvious advantage of not requiring a pressure calibration measurement.

Overlap Integral

The isolated effects of the overlap integral are shown in Figs. 12 and 13, based on the Doppler width associated with dye laser excitation of the (1,0) band. Since the Doppler widths (proportional to ν_a) for the XeCl and KrF pumped transitions differ from the (1,0) band by only ~10%, the results shown in the figures also apply in general to these other excitation options. As evidenced in Fig. 12, the overlap integral is sensitive to pressure, especially above 2 atm, but less sensitive for spectrally broader lasers.

Unlike the strong pressure dependence, Fig. 13 shows that the overlap integral varies little over a broad temperature range, for a 0.5-cm^{-1} laser. With more narrow bandwidths, the variations grow. The small change at 1 atm is a result of the counterbalancing effects of Doppler and collision broadening.

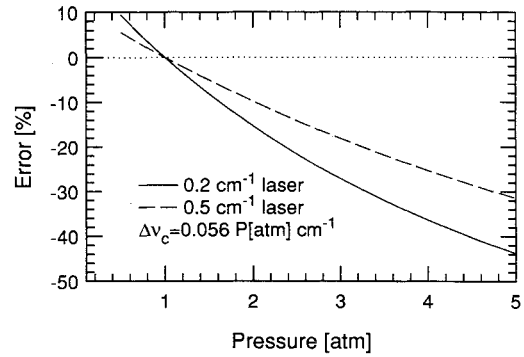

Fig. 12 Pressure-related systematic errors associated with the overlap integral for dye (1,0) excitation at 1800 K, shown for two laser (FWHM) bandwidths ($\Delta\nu_c$ is the collision-broadening width for products of a stoichiometric H_2-air flame[10]).

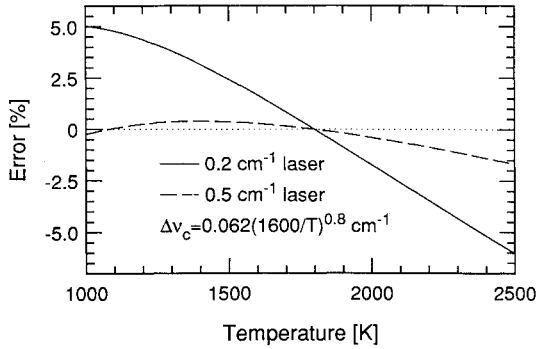

Fig. 13 Temperature-related systematic errors associated with the overlap integral for dye (1,0) excitation at 1 atm (the temperature scaling[10] for $\Delta\nu_c$ is also shown).

At 5 atm, the effect increases to ±10%, for the 0.5-cm^{-1} laser. As an additional error source, consider the pulse-to-pulse variations in laser bandwidth. For ±10% variations in the nominal 0.5-cm^{-1} laser width, the error in OH concentration is ±7% if no corrections are attempted, and the error is ±3% for a $1/\Delta\nu_{las}$ scaling [Eq. (1)].

Summary

A collection of the results is listed in Table 2. Dye laser pumping of the (1,0) band and KrF pumping of the (3,0) band exhibit relatively low systematic errors. XeCl pumping of the (0,0) band involves relatively large errors. The table also includes the random error (1/SNR) for two conditions: the calibration concentration of OH (2.4×10^{16} cm^{-3}, or 5000 ppm at 1500 K and 1 atm) and 10% of this value (500 ppm) to indicate dynamic range limits. As suggested by the earlier analysis (Table 1), XeCl excitation can produce very high signal levels, while single-shot images produced with KrF pumping will contain excessive random errors. Dye pumping provides a reasonable compromise between these two extremes. The errors listed in the table are based on values of $R=10^{10}$ s^{-1} and $Q_{e5}/Q_e=0.5$, but variations of R from 0.2 to 5×10^{10} s^{-1} and Q_{e5}/Q_e from 0 to 0.9 do not significantly alter the comparison.

Conclusions

For quantitative OH imaging and the study of large organized structures in turbulent combustion, single-shot imaging with good spatial resolution is required. Under these constraints, dye laser excitation of the (1,0) band of OH appears to be the best approach, compared to XeCl excimer pumping of the (0,0) band and KrF pumping of the (3,0) band. In many of these flames, quench rates appear to vary by less than 10% in regions of significant OH concentration. Nonlinear responses to changes in laser energy, population fraction, and pressure effects related to saturation and depletion are within this range for dye laser excitation of the (1,0) band. To stay within these limits, however, the output of some dye laser systems may have to be reduced below the maximum available energy. Use of a dye laser also allows the greatest flexibility in choosing excitation transitions optimized for a specific flow condition. For example, a line with a lower absorption coefficient can be chosen when laser absorption is a problem. Combined with the excess available laser energy, this can result in no loss of signal.

Because of the extremely low B coefficients for excitation of the (3,0) band, the KrF laser does not significantly perturb the absorbing state population. Even low rotational transfer rates can maintain the population of the laser excited rotational level. Unfortunately, the low fluorescence signals preclude meaningful single-shot images. For situations where only average flowfield data is required, frame averaging many images will significantly reduce the random error.

XeCl excitation produces bright, low-noise images, which permits measurements of large flowfields and application of a number of image processing methods.[18] The increased laser energy available in the XeCl laser, compared to typical dye lasers, is capable of approaching saturation conditions, thus reducing the laser energy and quenching dependences of the fluorescence. The quenching dependence can be further reduced with very fast detector gates. Unfortunately, saturation

Table 2 Systematic and random (noise) errors associated with OH PLIF

Laser	N_p, model	Systematic error, % E^a	$f_1{}^b$	P^c	$N_p{}^d$ (E_{cal}/2) photons	SNR^{-1}, % $n_{OH,cal}$ $K=2$	SNR^{-1}, % $n_{OH,cal}/10$ $K=2$
Dye	$\propto Ef_1/P$	±8	±5	±15	17,000	±3.4	±11
KrF	$\propto Ef_1$	±2	±2	±29	190	±32	±100
XeCl	$\propto f_1/P$	±34	±36	±20	190,000	±1.0	±3.2
Gated XeCl	$\propto f_1$	±38	±26	±44	110,000	±1.3	±4.2

[a] $E/E_{cal}=0.25$–1. [b] $f_1/f_{1,cal}$ for 700–2500 K. [c] $P/P_{cal}=0.5$–5. [d] Detection constants from Table 1.

combined with depletion makes the fluorescence a nonlinear function of population fraction (f_1). While this obstacle could be reduced by choosing an absorbing rotational level with nearly temperature-independent population fraction, no such transition exists within the limited tuning range of the XeCl laser for temperatures within the range 700–2500 K (or even for more limited ranges such as 1000–2000 K).

For quantitative OH imaging with relatively broadband lasers, uncorrected variations in the spectral overlap integral are a significant source of error at high pressures or when there are large variations in the laser spectral width. In the latter case, corrections can be performed by monitoring the laser linewidth.

There are a number of other aspects of quantitative PLIF imaging which require further examination. These include the effects of rotation-level and vibration-level dependent collision and predissociation rates, laser absorption, fluorescence trapping, and laser-created interferences. For example, the high intensities of ultraviolet excimer lasers can cause damage to "dirty" combustor windows or produce fluorescence of photodissociated hydrocarbon species.

Acknowledgments

This work was supported by the U.S. Air Force Office of Scientific Research, Aerospace Sciences Directorate, with J. Tishkoff as technical monitor. The authors acknowledge the assistance of M. P. Lee.

References

[1]Hanson, R. K., "Combustion Diagnostics: Planar Flowfield Imaging," *Twenty-First Symposium (International) on Combustion,* Combustion Inst., Pittsburgh, PA, 1987, pp. 1677–1691.

[2]Hanson, R. K., Seitzman, J. M., and Paul, P. H., "Planar Laser-Fluorescence Imaging of Combustion Gases," *Applied Physics B,* Vol. 50, No. 6, 1990, pp. 441–454.

[3]Stepowski, D., and Cottereau, M. J., "Study of the Collisional Lifetime of Hydroxyl ($^2\Sigma^+$, $v' = 0$) Radicals in Flames by Time-Resolved Laser-Induced Fluorescence," *Combustion and Flame,* Vol. 40, No. 1, 1981, pp. 65–70.

[4]Allen, M. G., "Digital Imaging Techniques for Single- and Multi-Phase Reacting Flowfields," Ph.D. Dissertation, Dept. of Mechanical Engineering, Stanford Univ., Stanford, CA, April 1987.

[5]Barlow, R. S., and Collignon, A., "Linear LIF Measurements of OH in Nonpremixed Methane-Air Flames: When are Quenching Corrections Unnecessary," AIAA Paper 91-0179, Jan. 1991.

[6]Cattolica, R. J., "OH Rotational Temperature From Two-Line Laser-Excited Fluorescence," *Applied Optics,* Vol. 20, No. 7, 1981, pp. 1156–1166.

[7]Hiller, B., and Hanson, R. K., "Simultaneous Planar Measurements of Velocity and Pressure Fields in Gas Flows Using Laser-Induced Fluorescence," *Applied Optics,* Vol. 27, No. 1, 1988, pp. 33–48.

[8]Berg, J. O., and Shackleford, W. L., "Rotational Redistribution Effect on Saturated Laser-Induced Fluorescence," *Applied Optics,* Vol. 18, No. 13, 1979, pp. 2093–2094.

[9]Lucht, R. P., Sweeney, D. W., and Laurendeau, N. M., "Balanced Cross-Rate Model for Saturated Molecular Fluorescence in Flames Using a Nanosecond Pulse Length Laser," *Applied Optics,* Vol. 19, No. 19, 1980, pp. 3295–3300.

[10]Rea, E. C., Jr., "Rapid-Tuning Laser Wavelength Modulation Spectroscopy with Applications in Combustion Diagnostics and OH Line Shape Studies," Ph.D. Dissertation, Dept. of Mechanical Engineering, Stanford Univ., Stanford, CA, Dec. 1990.

[11]Greenstein, H., and Bates, C. W., Jr., "Line-Width and Tuning Effects in Resonant Excitation," *Journal of the Optical Society of America,* Vol. 65, No. 1, 1975, pp. 33–40.

[12]Hanson, R. K., and Seitzman, J. M., "Planar Fluorescence Imaging in Gases," *Experimental Methods for Flows with Combustion,* edited by A. Taylor, Academic Press, London, 1993, Chap. 6.

[13]Chidsley, I. L., and Crosley, D. R., "Calculated Rotational Transition Probabilities for the A-X System of OH," *Journal of Quantitative Spectroscopy and Radiative Transfer,* Vol. 23, No. 2, 1980, pp. 187–189.

[14]Kychakoff, G., Howe, R. D., Hanson, R. K., and McDaniel, J. C., "Quantitative Visualization of Combustion Species in a Plane," *Applied Optics,* Vol. 21, No. 18, 1982, pp. 3225–3227.

[15]Dyer, M. J., and Crosley, D. R., "Two-Dimensional Imaging of OH Laser-Induced Fluorescence in a Flame," *Optics Letters,* Vol. 7, No. 8, 1982, pp. 382–384.

[16]Allen, M. G., and Hanson, R. K., "Digital Imaging of Species Concentration Fields in Spray Flames," *Twenty-First Symposium (International) on Combustion,* Combustion Inst., Pittsburgh, PA, 1987, pp. 1755–1761.

[17]Andresen, P., Bat, A., Gröger, W., Lülf, H. W., Meijer, G., and ter Meulen, J. J., "Laser-Induced Fluorescence with Tunable Excimer Lasers as a Possible Method for Instantaneous Temperature Field Measurements at High Pressures: Checks with an Atmospheric Pressure Flame," *Applied Optics,* Vol. 27, No. 2, 1988, pp. 365–378.

[18]Seitzman, J. M., Üngüt, A., Paul, P. H., and Hanson, R. K., "PLIF Imaging Analysis of OH Structures in a Turbulent Nonpremixed H_2-Air Flame," AIAA Paper 90-0160, Jan. 1990.

[19]Gray, J. A., and Farrow, R. L., "Predissociation Lifetimes of OH $A^2\Sigma^+(v' = 3)$ Obtained From Optical-Optical Double-Resonance Linewidth Measurements," *Journal of Chemical Physics,* Vol. 95, No. 10, 1991, pp. 7054–7060.

[20]Massey, G. A., and Lemon, C. J., "Feasibility of Measuring Temperature and Density Fluctuations in Air Using Laser-Induced O_2 Fluorescence," *Journal of Quantum Electronics,* Vol. 20, No. 5, 1984, pp. 454–457.

[21]Lee, M. P., and Hanson, R. K., "Calculations of O_2 Absorption and Fluorescence at Elevated Temperatures for a Broadband Argon Fluoride Laser Source at 193 nm," *Journal of Quantitative Spectroscopy and Radiative Transfer,* Vol. 36, No. 5, 1986, pp. 425–440.

[22]Meijer, G., ter Meulen, J. J., Andresen, P., and Bath, A., "Sensitive Quantum State Selective Detection of H_2O and D_2O by (2 + 1) Resonance Enhanced Multiphoton Ionization," *Journal of Chemical Physics,* Vol. 85, No. 12, 1986, pp. 6914–6922.

[23]Lucht, R. P., Sweeney, D. W., and Laurendeau, N. M., "Time-Resolved Fluorescence Investigation of Rotational Transfer in $A^2\Sigma^+(v = 0)$ OH," *Applied Optics,* Vol. 25, No. 22, 1986, pp. 4086–4095.

[24]Carter, C. D., Salmon, J. T., King, G. B., and Laurendeau, N. M., "Feasibility of Hydroxyl Concentration Measurements by Laser-Saturated Fluorescence in High-Pressure Flames," *Applied Optics,* Vol. 26, No. 21, 1987, pp. 4551–4562.